Tensor Asymmetry A_{zz} in the $x > 1$ Region

A Proposal to Jefferson Lab PAC 42

E. Long, [†] [‡] K. Slifer,[†] P. Solvignon[†]
University of New Hampshire, Durham, NH 03861

D. Day,[†] D. Keller[†]
University of Virginia, Charlottesville, VA 22903

D. Higinbotham[†]
Thomas Jefferson National Accelerator Facility, Newport News, VA 23606

M. Strikman
Pennsylvania State University, University Park, PA 16802

[†]Spokesperson
[‡]Contact: ellie@jlab.org

Abstract

The tensor-polarized target asymmetry, A_{zz}, which is used to extract b_1 in the DIS region through the D(e, e')X channel, can be used to extract information on nucleon-nucleon interactions in the quasi-elastic region. The reaction is unique in that it can probe color transparency, which has never been explored at Jefferson Lab, and improve understanding of the deuteron wave function and particularly probe how short range correlations arise from proton-neutron interactions.

In the quasi-elastic region, A_{zz} was first calculated in 1988 by Frankfurt and Strikman, using the Hamada-Johnstone and Reid soft-core wave functions [1]. Recent calculations by M. Sargsian revisit A_{zz} in the $x > 1$ range using virtual-nucleon and light-cone methods, which differ by up to a factor of two [2].

An experimental determination of A_{zz} could be performed utilizing equipment identical for E13-12-011 at five different Q^2 values over the course of 24 days, with [NUMBER] additional days of commissioning. The measurements are less sensitive to the target polarization than E13-12-011, such that this experiment could be used to prove that the condition of 30% in-beam polarization is met for E13-12-011.

Contents

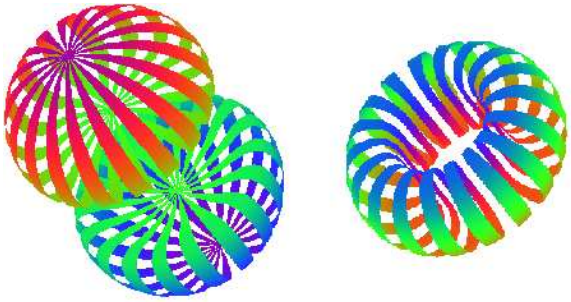

Figure 1: Equidensity lines of the deuteron in its two spin projections, $M_J = \pm 1$ and $M_J = 0$, respectively. Reproduced from [3, 4].

1 Background and Motivation

The deuteron is the simplest composite nuclear system, and in many ways it is as important to understanding bound states in QCD as the hydrogen atom was to understanding bound systems in QED. Our experimental and theoretical understanding of the deuteron remains unsatisfying. By taking a ratio of electron scattering off of tensor-polarized and unpolarized deuterons, the S- and D-wave states can be disentangled, leading to a fuller understanding of the repulsive nucleon core.

Understanding the nucleon-nucleon potential of the deuteron is essential for understanding short-range correlations. To resolve the short-range structure of nuclei on the level of nucleon and hadronic constituents, we need processes that transfer to the nucleon constituents both energy and momentum larger than the scale of the NN short range correlations. By scanning over a large range of Q^2, we can measure how these processes begin to dominate the tensor asymmetry A_{zz}.

1.1 Deuteron Wavefunction

1.2 Separating the Deuteron S- and D-States

It was suggested for some time that to resolve the microscopic structure of nuclei one needs to study scattering at sufficiently large momentum transfer and large relative momenta of the produced nucleons. Effectiveness of this logic was confirmed by a series of the experiments at BNL and JLab which directly observed short-range correlations (SRC) in a series of nuclei and established similarity of the SRC in the deuteron and heavier nuclei with pn correlations giving dominant contribution. Hence, deuteron serves as a "hydrogen atom" for the studies of the microscopic short-range structure of the nuclei.

Thus to achieve further progress of the field it is necessary to improve our knowledge of the deuteron wave function at high momenta and especially to separate contribution to the high momentum component of the deuteron, the contribution of S- and D-waves. Note here that the dominance of the D-wave at large range of the nucleon momenta is expected in a range of the theoretical models but experimentally it was probed in a rather indirect way via measurement of T_{20} for the deuteron form factor. Still the knowledge of S/D ratio for large momenta is rather poor. Indeed all wavefunctions are constrained by low energy date to reproduce S/D ratio at small momenta while

the overall probability of the D-wave in the deuteron differs by a factor up to 1.5, leading to a large difference of the S/D ratio at large momenta.

The experience with the studies of the ratios of the (e, e) cross sections at $x > 1$ has demonstrated an early onset of the scaling of the ratios when plotted as a function of the light-cone fraction of the struck nucleon momentum. As a result, the ratios were providing a direct measure of the ratio of the high momentum components in nuclei. Similarly, one can expect that in the case of scattering of the polarized deuteron we expect the early scaling for the asymmetry when plotted as a function of the minimal struck nucleon momentum or the light cone fraction in the A(e, e) case. It was observed at JLab that the scaling of the ratios is setting in starting at $Q^2 \sim 1\ \mathrm{GeV}^2$ so covering the range of Q^2 up to 2 GeV^2 should be sufficient to measure the S/D ratios in an interesting momentum range.

It is worth noting here that on the top of comparing predictions for the different wave functions, one expects to be able to distinguish between non-relativistic and light cone quantum mechanic models. The principal difference between the models is the relation between the spectator momentum and momentum in the wave function - in the nonrelativistic model they coincide, while in the light cone model the relation is non-linear starting at $k \sim 250\ \mathrm{MeV}/c$. This difference is most clearly manifested in the scattering off the polarized deuteron due to a strong dependence of the S/D ratio on the nucleon momentum.

1.3 Tensor Asymmetry Azz

The S- and D-states are to the tensor asymmetry A_{zz} by [1]

$$A_{zz} \propto \frac{u(k)w(k)\sqrt{2} + \frac{1}{2}w^2(k)}{u^2(k) + w^2(k)}, \tag{1}$$

where $u(k)$ is the ${}^3S_1$ wave function and $w(k)$ is the ${}^3D_1$ wave function.

For decades [5], it has been known that the nucleon-nucleon potential has a short-range repulsive core, which is responsible for the stability of strongly interacting matter. However, a description of the repulsive core remains largely unconstrained and our understanding of QCD dynamics at short distances (≤ 0.5 fm) largely incomplete [6].

Due to their small size [**?**] and simple structure, tensor polarized deuterons are ideal for studying nucleon-nucleon interactions. Tensor polarization enhances the D-state wavefunction, which compresses the deuteron from $\sim?$ fm to ~ 0.5 fm [4] and has been noted to be revealing of short-range QCD effects.

2 The Proposed Experiment

2.1 Experimental Method

As in the case for E12-13-011, the measured double differential cross section for a spin-1 target characterized by a vector polarization P_z and tensor polarization P_{zz} is expressed as,

$$\frac{d^2\sigma_p}{d\Omega dE'} = \frac{d^2\sigma_u}{d\Omega dE'}\left(1 - P_z P_B A_1 + \frac{1}{2}P_{zz}A_{zz}\right), \tag{2}$$

where, σ_p (σ_u) is the polarized (unpolarized) cross section, P_B is the incident electron beam polarization, and A_1 (A_{zz}) is the vector (tensor) asymmetry of the virtual-photon deuteron cross section. This allows us to write the polarized tensor asymmetry with $0 < P_{zz} \leq 1$ using an unpolarized electron beam as

$$A_{zz} = \frac{2}{P_{zz}}\left(\frac{\sigma_p - \sigma_u}{\sigma_u}\right), \tag{3}$$

where σ_p is the polarized cross section. The tensor polarization is given by

$$P_{zz} = \frac{n_+ - 2n_0 + n_-}{n_+ + n_- + n_0}, \tag{4}$$

where n_m represents the population in the $m_z = +1$, -1, or 0 state.

Eq. 3 reveals that the asymmetry A_{zz} compares two different cross sections measured under different polarization conditions of the target: positively tensor polarized and unpolarized. To obtain the relative cross section measurement in the same configuration, the same target cup and material will be used at alternating polarization states (polarized vs. unpolarized), and the magnetic field providing the quantization axis will be oriented along the beamline at all times. This field will always be held at the same value, regardless of the target material polarization state. This process, identical to that used for the E12-13-011 b_1 measurement, ensures that the acceptance remains consistent within the stability (10^{-4}) of the super conducting magnet.

Since many of the factors involved in the cross sections cancel in the ratio, Eq. 3 can be expressed in terms of the charge normalized, efficiency corrected numbers of tensor polarized (N_p) and unpolarized (N_u) counts,

$$A_{zz} = \frac{2}{fP_{zz}}\left(\frac{N_p - N_u}{N_u}\right). \tag{5}$$

The dilution factor f corrects for the presence of unpolarized nuclei in the target and is defined by

$$f = \frac{N_D\sigma_D}{N_N\sigma_N + N_D\sigma_D + \sum_A N_A\sigma_A}, \tag{6}$$

where N_D is the number of deuterium nuclei in the target and σ_D is the corresponding inclusive double differential scattering cross section, N_N is the nitrogen number of scattered nuclei with

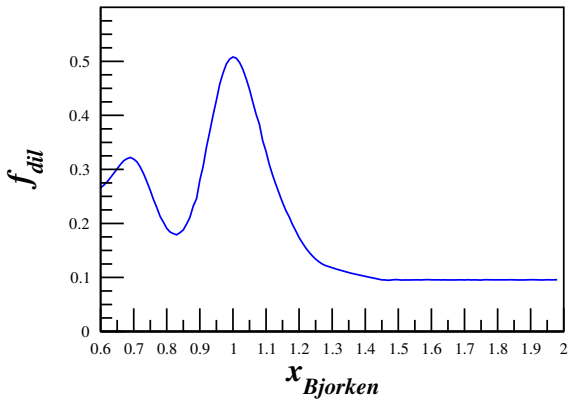

Figure 2: The estimated dilution factor, in this case at $Q^2 = 1.5\ (\mathrm{GeV}/c)^2$, is expected to drop off at high x until it reaches the SRC plateau region. This effect will be counteracted by using a high-luminosity solid target.

cross section σ_N, and N_A is the number of other scattering nuclei of mass number A with cross section σ_A. As has been noted in previous work [1], the dilution factor at high x drops off considerably until the SRC plateau region, as shown in Fig. 2. By using a high-luminosity solid target and a low angle $\theta_{e'}$, this effect will be largely counteracted.

The dilution factor can be written in terms of the relative volume ratio of ND_3 to LHe in the target cell, otherwise known as the packing fraction p_f. In our case of a cylindrical target cell oriented along the magnetic field,the packing fraction is exactly equivalent to the percentage of the cell length filled with ND_3.

If the time is evenly split between scattering off of polarized and unpolarized ND_3, the time necessary to achieve the desired precision δA is:

$$T = \frac{N_p}{R_p} + \frac{N_u}{R_u} = \frac{8}{f^2 P_{zz}^2}\left(\frac{R_p(R_u + R_p)}{R_u^3}\right)\frac{1}{\delta A_{zz}^2} \tag{7}$$

where $R_{p(u)}$ is the polarized (unpolarized) rate and $N_{p(u)}$ is the total estimated number of polarized (unpolarized) counts to achieve the uncertainty δA_{zz}.

2.1.1 Statistical Uncertainty

To investigate the statistical uncertainty we start with the equation for A_{zz} using measured counts for polarized data (N_p) and unpolarized data (N_u),

$$A_{zz} = \frac{2}{f P_{zz}}\left(\frac{N_p}{N_u} - 1\right). \tag{8}$$

The statistical error with respect to counts is then

$$\delta A_{zz} = \frac{2}{f P_{zz}}\sqrt{\left(\frac{\delta N_p}{N_u}\right)^2 + \left(\frac{N_p \delta N_u}{N_u^2}\right)^2}. \tag{9}$$

Source	Systematic
Polarimetry	7.7%
Dilution/packing fraction	4.0%
Radiative corrections	1.5%
Charge Determination	1.0%
Detector resolution and efficiency	1.0%
Total	10%

Table 1: Estimates of the scale dependent contributions to the systematic error of A_{zz}.

For $\delta N_{p(u)} = \sqrt{N_{p(u)}}$, the uncertainty becomes

$$\delta A_{zz} = \frac{2}{f P_{zz}} \sqrt{\frac{N_p(N_u + N_p)}{N_u^3}}, \tag{10}$$

which can't be simplified further due to the large expected asymmetry.

2.1.2 Systematic Uncertainty

Table 1 shows a list of the scale dependent uncertainties contributing to the systematic error in A_{zz}.

With careful minimization, the uncertainty in P_z can be held to better than 4%, as demonstrated in the recent g2p/GEp experiment [7]. This leads to a a relative uncertainty in P_{zz} of 7.7%. Alternatively, the tensor asymmetry can be directly extracted from the NMR lineshape as discussed in Sec. 2.3, with similar uncertainty. The uncertainty from the dilution factor and packing fraction of the ammonia target contributes at the 4% level. The systematic effect on A_{zz} due to the QED radiative corrections will be quite small. For our measurement there will be no polarized radiative corrections at the lepton vertex, and the unpolarized corrections are known to better than 1.5%.

Charge calibration and detector efficiencies are expected to be known better to 1%, but the impact of time-dependent drifts in these quantities must be carefully controlled.

Time dependent factors

Eq. 5 involves the ratio of counts, which leads to cancellation of several first order systematic effects. However, the fact that the two data sets will not be taken simultaneously leads to a sensitivity to time dependent variations which will need to be carefully monitored and suppressed. To investigate the systematic differences in the time dependent components of the ntegrated counts, we need to consider the effects from calibration, efficiency, acceptance, and luminosity between the two polarization states.

Fluctuations in luminosity due to target density variation can easily be kept to a minimum by keeping the material beads at the same temperature for both polarization states by control of the microwave and the LHe evaporation. The He vapor pressure reading can give accuracy of material temperature changes at the level of $\sim$0.1%. Beam rastering can also be controlled to a high degree.

The acceptance of each cup can only change as a function of time if the magnetic field changes. The capacity to set, reset, and hold the target superconducting magnet to a desired holding field causes a field uncertainty of only $\delta B/B = 0.01\%$. This implies that, like the cup length l, the acceptance $\mathcal{A}$ for each polarization state is the same.

In order to look at the effect on A_{zz} due to drifts in beam current monitor calibration and detector efficiency, we rewrite Eq. 5 explicitly in terms of the raw measured counts N_p^c and N_u^c,

$$\begin{aligned} A_{zz} &= \frac{2}{fP_{zz}}\left(\frac{N_p^c}{N_u^c} - 1\right) \\ &= \frac{2}{fP_{zz}}\left(\frac{Q\varepsilon l\mathcal{A}}{Q_1\varepsilon_1 l\mathcal{A}}\frac{N_p}{N_u} - 1\right) \end{aligned} \tag{11}$$

where Q represents the accumulated charge, and ε is the detector efficiency. The target length l and acceptance $\mathcal{A}$ are identical in both states to first order.

We can then express Q_1 as the change in beam current measurement calibration that occurs in the time it takes to collect data in one polarization state before switching to another, such that $Q_1 = Q(1 - dQ)$. In this notation dQ is a dimensionless ratio of changes in different polarization states. A similar representation is used for drifts in detector efficiency leading to,

$$A_{zz} = \frac{2}{fP_{zz}}\left(\frac{N_pQ(1-dQ)\varepsilon(1-d\varepsilon)}{N_uQ\varepsilon} - 1\right). \tag{12}$$

which simplifies to,

$$A_{zz} = \frac{2}{fP_{zz}}\left(\frac{N_p}{N_u}(1 - dQ - d\varepsilon + dQd\varepsilon) - 1\right). \tag{13}$$

For estimates of the dQ and $d\varepsilon$ we turn to previous experimental studies. For HRS detector drift during the JLab transversity experiment E06-010, the detector response was measured such that the normalized yield for same condition over a three month period indicated little change ($< 1\%$). These measurement were then used to show that for short time (20 minutes periods between target spin flip), the detector drift was estimated to be less than 1% times the ratio of the time period between target spin flip and three months. For the present experiment we use the same estimate except for the period between target polarization states used is $\sim$12 hours leading to an overall drift $d\varepsilon \sim 0.01\%$. A similar approach can be used to establish an estimate for dQ using studies from the data from the (g2p/GEp) experiment resulting in $d\varepsilon \sim 0.01\%$.

To express A_{zz} in terms of the estimated experimental drifts in efficiency and current measurement we can write,

$$A_{zz} = \frac{2}{fP_{zz}}\left(\frac{N_1}{N} - 1\right) \pm \frac{2}{fP_{zz}}d\xi. \tag{14}$$

This leads to a contribution to A_{zz} on the order of 1×10^{-3},

$$dA_{zz}^{drift} = \pm\frac{2}{fP_{zz}}d\xi = \pm 3.7 \times 10^{-3}. \tag{15}$$

Though a very important contribution to the error this value allows a clean measurement of $A_{zz} = 0$ at $x = 0.45$ without overlap with the Hermes error bar. For this estimate we assume only two

	E_0 (GeV)	Q^2 (GeV^2)	W (GeV)	E' (GeV)	$\theta_{e'}$ (deg.)	Rates (kHz)	PAC Time (hours)
SHMS	8.8	1.5	0.46	8.36	8.2	0.55	600
SHMS	6.6	0.7	0.60	6.50	8.2	4.08	90
SHMS	2.2	0.3	0.87	2.11	14.4	3.73	30
HMS	2.2	0.3	0.86	2.11	14.9	4.65	30

Table 2: Summary of the kinematics and physics rates using the Hall C spectrometers.

polarization state changes in a day. If it is possible to increase this rate then the systematic effect in A_{zz} will decrease accordingly.

Naturally detector efficiency can drift for a variety of reasons, for example including fluctuations in gas quality, HV drift or drifts in the spectrometers magnetic field. All of these types of variation as can be realized both during the experiment though monitoring as well as systematic studies of the data collected.

It can be difficult to know changes in luminosity, however the identical condition of the two polarization states minimizes the relative changes in time. There are also checks on the consistency of the cross section data that can be use ensuring the quality of each run used in the asymmetry analysis. Each of these systematic effects can mitigate the systematic uncertainty to ~ 0.001, which is required for the b_1 measurement. In the kinematic region proposed here, A_{zz} is expected to be much larger, on the order of 0.1 to 1.0. While typical false asymmetries in Hall C of 0.01 are acceptable for this proposed measurement, it can also allow for a test of the methods used to reduce them further.

2.2 Kinematics

We will measure the tensor asymmetry A_{zz} for $0.80 < x < 1.75$, 1.0 (GeV/c)^2 $< Q^2 <$ 1.9 (GeV/c)^2, and $0.59 < W < 1.09$ GeV. Fig. 3 shows the planned kinematic coverage utilizing the Hall C HMS and SHMS spectrometers at forward angle.

The polarized ND_3 target is discussed in section 2.3. The magnetic field of the target will be held constant along the beamline at all times, while the target state is alternated between a polarized and unpolarized state. The tensor polarization and packing fraction used in the rates estimate are 30% and 0.65 , respectively. The dilution fraction changes with x in the range of this measurement as shown in Fig. 4. With an incident electron beam current of 115 nA, the expected deuteron luminosity is $?.?? \times 10^{35}$ cm^{-2}s^{-1}.

The momentum bite and the acceptance were assumed to be $\Delta P = \pm 8\%$ and $\Delta\Omega = 5.6$ msr for the HMS, and $\Delta P = ^{+20\%}_{-8\%}$ and $\Delta\Omega = 4.4$ msr for the SHMS. For the choice of the kinematics, special attention was taken onto the angular and momentum limits of the spectrometers: for the HMS, $10.5^\circ \leq \theta \leq 85^\circ$ and $1 \leq P_0 \leq 7.3$ GeV/c, and for the SHMS, $5.5^\circ \leq \theta \leq 40^\circ$ and $2 \leq P_0 \leq 11$ GeV/c. In addition, the opening angle between the spectrometers is physically constrained to be larger than 17.5°. The dilution factors and projected uncertainties in A_{zz} are

	$Q^2 = 1.5$ (GeV/c)^2			$Q^2 = 0.7$ (GeV/c)^2			$Q^2 = 0.3$ (GeV/c)^2		
x	f_{dil}	δA_{zz}^{stat} $\times 10^{-2}$	δA_{zz}^{sys} $\times 10^{-2}$	f_{dil}	δA_{zz}^{stat} $\times 10^{-2}$	δA_{zz}^{sys} $\times 10^{-2}$	f_{dil}	δA_{zz}^{stat} $\times 10^{-2}$	δA_{zz}^{sys} $\times 10^{-2}$
0.80	0.205	0.52	0.53	0.175	0.63	0.53	0.298	0.41	0.53
0.90	0.274	0.39	1.20	0.375	0.27	1.20	0.462	0.25	1.20
1.00	0.507	0.21	0.05	0.518	0.19	0.05	0.521	0.24	0.01
1.10	0.333	0.42	1.75	0.409	0.31	1.42	0.431	0.35	1.16
1.20	0.174	1.13	3.51	0.264	0.66	2.85	0.301	0.65	2.32
1.30	0.120	2.32	5.26	0.174	1.26	4.27	0.193	1.18	3.48
1.40	0.127	3.61	7.01	0.156	2.18	5.69	0.144	1.91	4.64
1.50	0.096	5.81	8.77	0.170	2.93	7.12	0.100	3.19	5.81
1.60	0.096	7.93	10.0	0.110	4.86	8.54	0.086	4.09	6.97
1.70	0.095	10.7	10.0	0.096	6.97	9.96	0.063	6.30	8.31
1.80	0.096	13.7	10.0	0.096	9.13	10.0	0.056	7.72	9.29

Table 3: Summary of the expected statistical uncertainty after combining overlapping x-bins. Values represent the statistics weighted average of all events that satisfy our kinematic cuts.

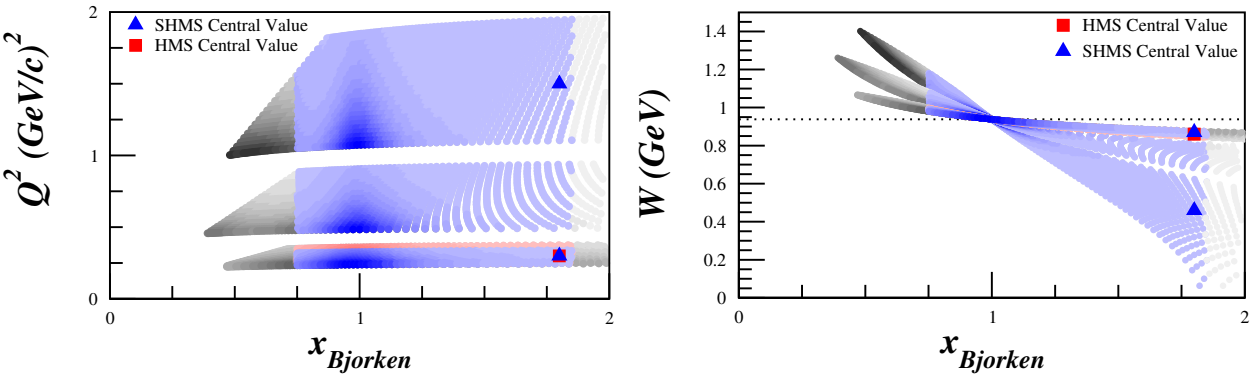

Figure 3: Kinematic coverage. The grey settings are not included in our rates estimates since they fall outside of $0.80 < x < 1.75$. The highlighted represent the central value of the spectrometer setting, which are not the statistics weighted average of the distribution. The shading represents areas with relative statistics for each setting.

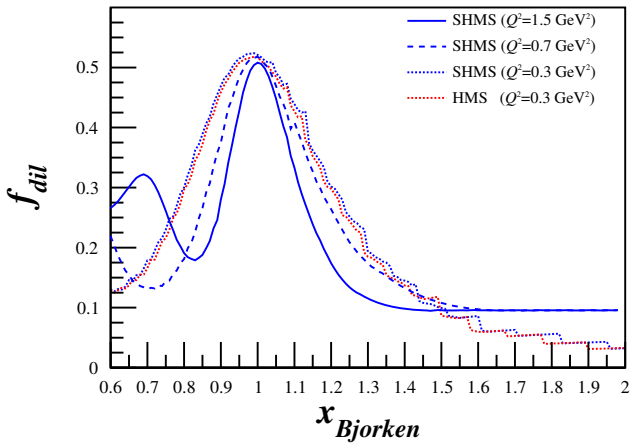

Figure 4: Projected dilution fraction covering the entire x range to be measured using a combination of the Bosted [8] and Sargsian [**?**] code for the SHMS and HMS.

summarized in Table 3 and displayed in Fig. 5.

A total of 30 days of beam time is requested for production data, with an additional 5 days of expected overhead.

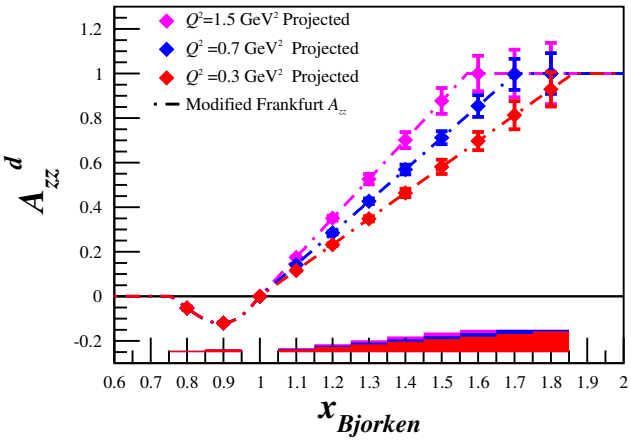

Figure 5: Projected statistical errors for the tensor asymmetry A_{zz} with 30 days of beam time. The band represents the systematic uncertainty. Also shown is the Frankfurt and Strikman model [1] that has been modified to estimate the plateau changing with Q^2.

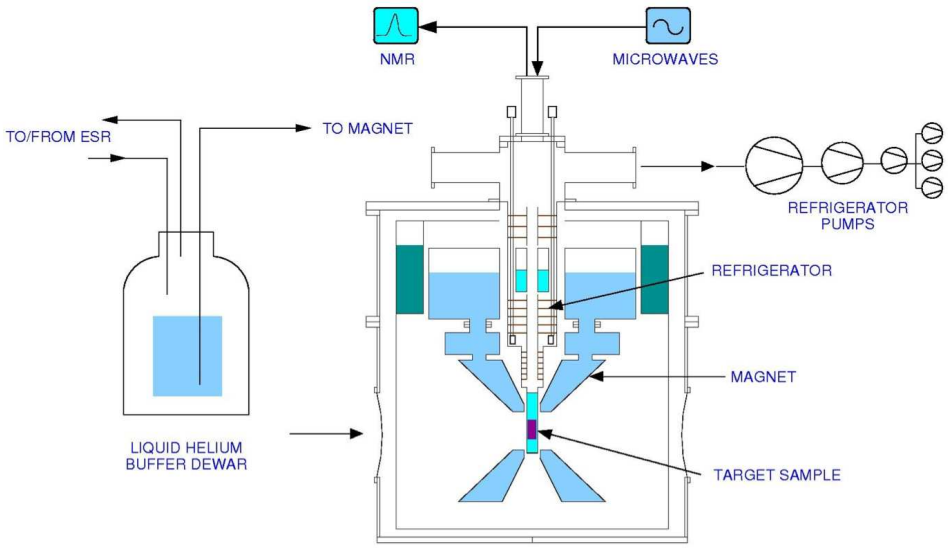

Figure 6: Cross section view of the JLab/UVa polarized target. Figure courtesy of C. Keith.

2.3 Polarized Target

This experiment will use the JLab/UVa dynamically polarized solid ND_3 target operated in longitudinal mode. The target is typically operated with a specialized slow raster and beamline instrumentation capable of characterizing the low current 50-100 nA beam. All of these requirements have been met previously in Hall C. The polarized target (see Fig. 6), has been successfully used in experiments E143, E155, and E155x at SLAC, and E93-026, E01-006 and E07-003, E08-027 and E08-007 at JLab. A similar target was used in Hall B for the EG1, EG4, and DVCS experiments.

The JLab/UVa target underwent significant renovation and improvement [9] during the recent g2p run. The magnet was replaced early in the run, and the target then performed consistently at or above historical levels. A new 1 K refrigerator and target insert were designed and constructed by the JLab target group. The cryogenic pumping system has been overhauled. In particular, the older Alcatel 2060H rotary vane pumps have been replaced with new Pfeiffer DU065 magnetically coupled rotary vane pumps, and the pump controls are being refurbished. The target motion system has been rebuilt from scratch.

The target operates on the principle of Dynamic Nuclear Polarization, to enhance the low temperature (1 K), high magnetic field (5 T) polarization of solid materials by microwave pumping. The polarized target assembly contains several target cells of 3.0 cm length that can be selected individually by remote control to be located in the uniform field region of a superconducting Helmholtz pair. The permeable target cells are immersed in a vessel filled with liquid Helium and maintained at 1 K by use of a high power evaporation refrigerator. The coils have a 50° conical shaped aperture along the beam axis which allow for unobstructed forward scattering.

The target material is exposed to microwaves to drive the hyperfine transition which aligns the nucleon spins. The heating of the target by the beam causes a drop of a few percent in the polarization, and the polarization slowly decreases with time due to radiation damage. Most of

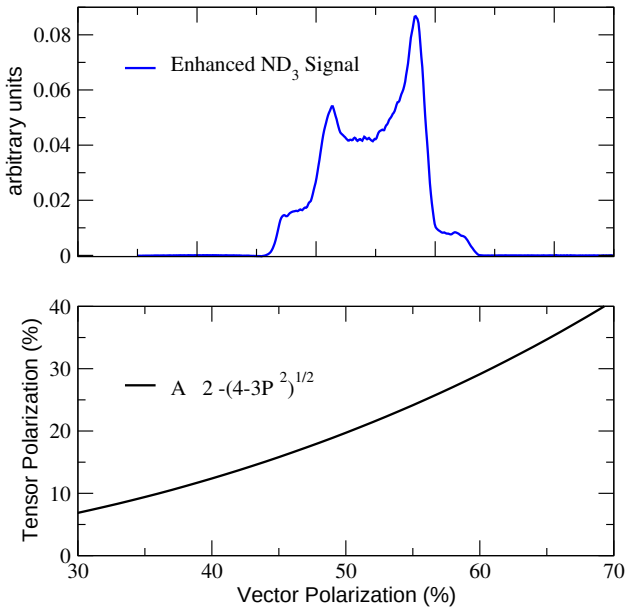

Figure 7: **Top**: NMR signal for ND_3 with a vector polarization of approximately 50% from the GEN experiment. **Bottom**: Relationship between vector and tensor polarization in equilibrium, and neglecting the small quadrupole interaction.

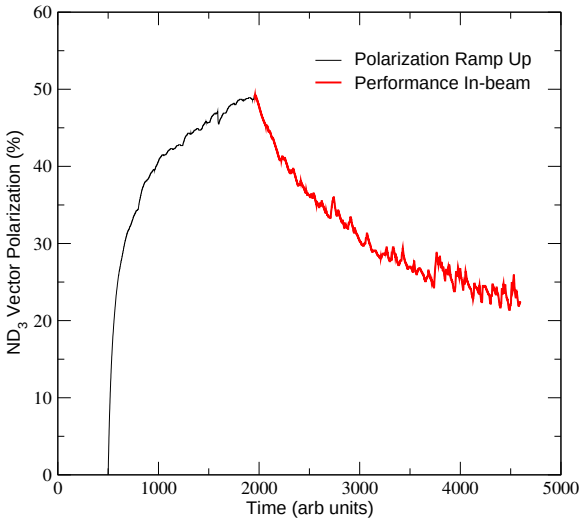

Figure 8: Performance of the ND_3 target during the GEN experiment.

the radiation damage can be repaired by periodically annealing the target, until the accumulated dose reached is greater than about 0.5×10^{17} e^-/cm^2, at which time the target material needs to be replaced.

2.3.1 Polarization Analysis

The three Zeeman sublevels of the deuteron system ($m = -1, 0, 1$) are shifted unevenly due to the quadrupole interaction [10]. This shift depends on the angle between the magnetic field and the electrical field gradient, and gives rise to two separate transition energies. Hence, the unique double peaked response displayed in Fig. 7. When the system is at thermal equilibrium with the solid lattice, the deuteron polarization is known from:

$$P_z = \frac{4 + \tanh \frac{\mu B}{2kT}}{3 + \tanh^2 \frac{\mu B}{2kT}} \tag{16}$$

where μ is the magnetic moment, and k is Boltzmann's constant. The vector polarization can be determined by comparing the enhanced signal with that of the TE signal (which has known polarization). This polarimetry method is typically reliable to about 5% relative.

Similarly, the tensor polarization is given by:

$$P_{zz} = \frac{4 + \tanh^2 \frac{\mu B}{2kT}}{3 + \tanh^2 \frac{\mu B}{2kT}} \tag{17}$$

From Eqs. 16 and 17, we find:

$$P_{zz} = 2 - \sqrt{4 - 3P_z^2}$$

In addition to the TE method, polarizations can be determined by analyzing NMR lineshapes as described in [11] with a typical 7% relative uncertainty. At high polarizations, the intensities of the two transitions differ, and the NMR signal shows an asymmetry R in the value of the two peaks, as shown in Fig. 7. The vector polarization is then given by:

$$P_z = \frac{R^2 - 1}{R^2 + R + 1} \tag{18}$$

and the tensor polarization is given by:

$$P_{zz} = \frac{R^2 - 2R + 1}{R^2 + R + 1} \tag{19}$$

The DNP technique produces deuteron vector polarizations of up to 60% in ND_3 and 64% in LiD [12], which corresponds to tensor polarizations of approximately 30%. The target polarization decays while in beam, so that the average vector polarization was about 35% in the GEN experiment, as seen if Fig. 8.

An average tensor polarization of 30% enables a significant measurement of $b_1(x)$, as shown in Fig. 5. Any improvement to the expected polarization, although not strictly necessary, would allow

the addition of kinematic points, and/or improved statistical accuracy. With this in mind, we are pursuing techniques to enhance the tensor polarization by directly stimulating transitions to/from the $M_s = 0$ state, as discussed in Ref. [10]. D. Crabb from the UVa group had some success in obtaining enhanced tensor polarizations via RF saturation of one of the Zeeman transitions, otherwise known as "hole-burning". The method was not pursued due to the lack of need for tensor polarized targets at the time of the study. Another method to enhance tensor polarization entails simultaneously pumping the sample with two independent microwave frequencies, which requires careful isolation of the respective cavities.

2.3.2 Depolarizing the Target

To move from polarized to unpolarized measurements, the target polarization will be annihilated using destructive NMR loop field changes and destructive DNP microwave pumping. It is also possible to remove LHe in the nose of the target to remove the polarization by heating. During unpolarized data taking the incident electron beam heating is enough to remove the thermal equilibrium polarization.

The NMR measurement will ensure zero polarization. The target material will be kept at $\sim$1 K for polarized and unpolarized data collection, and the target field will be held constant for both states as well. These consistencies are used to minimize the systematic differences in the polarized and unpolarized data collection. To minimize systematic effects over time, the polarization condition will be switched twice in a 24 hour period. This is expected to account for drift in integrated charge accumulation.

2.3.3 Rendering Dilution Factor

To derive the dilution factor, we first start with the ratio of polarized to unpolarized counts. In each case, the number of counts that are actually measured, neglecting the small contributions of the thin aluminium cup window materials, NMR coils, etc., are

$$N_1 = Q_1 \varepsilon_1 \mathcal{A}_1 l_1 [(\sigma_N + 3\sigma_1) p_f + \sigma_{He}(1 - p_f)], \tag{20}$$

and

$$N = Q \varepsilon \mathcal{A} l [(\sigma_N + 3\sigma) p_f + \sigma_{He}(1 - p_f)]. \tag{21}$$

where Q represents accumulated charge, ε is the dectector efficiency, $\mathcal{A}$ the cup acceptance, and l the cup length.

For this calculation we assume similar charge accumulation such that $Q \simeq Q_1$, and that the efficiencies stay constant, in which case all factors drop out of the ratio leading to

$$\begin{aligned}
\frac{N_1}{N} &= \frac{(\sigma_N + 3\sigma_1) p_f + \sigma_{He}(1 - p_f)}{(\sigma_N + 3\sigma) p_f + \sigma_{He}(1 - p_f)} \\
&= \frac{(\sigma_N + 3\sigma(1 + A_{zz} P_{zz}/2)) p_f + \sigma_{He}(1 - p_f)}{(\sigma_N + 3\sigma) p_f + \sigma_{He}(1 - p_f)} \\
&= \frac{[(\sigma_N + 3\sigma) p_f + \sigma_{He}(1 - p_f)] + 3\sigma A_{zz} P_{zz}/2}{(\sigma_N + 3\sigma) p_f + \sigma_{He}(1 - p_f)}
\end{aligned}$$

$$
\begin{aligned}
&= 1 + \frac{3\sigma A_{zz} P_{zz}/2}{(\sigma_N + 3\sigma) p_f + \sigma_{He}(1 - p_f)} \\
&= 1 + \frac{1}{2} f A_{zz} P_{zz}, \qquad (22)
\end{aligned}
$$

where $\sigma_1 = \sigma(1 + A_{zz}P_{zz}/2)$ has ben substituted, per Eq. 2, with $P_B = 0$. It can be seen that the above result corresponds to Eq. 5.

References

[1] L. Frankfurt and M. Strikman, Phys.Rept. **160**, 235 (1988).

[2] M. Sargsian, private communication, to be published.

[3] J. Carlson and R. Schiavilla, Rev. Mod. Phys. **70**, 743 (1998).

[4] J. L. Forest *et al.*, Phys. Rev. **C54**, 646 (1996).

[5] R. Jastrow, Phys. Rev. **81**, 165 (1951).

[6] M. M. Sargsian, (2014).

[7] D. Keller, "Uncertainty in DNP Target Data for E08-007", JLab-TN-12-051.

[8] P. Bosted and V. Mamyan, (2012).

[9] C. Keith, JLab polarized target group. Private communication.

[10] W. Meyer *et al.*, Nucl. Instrum. Meth. **A244**, 574 (1986).

[11] C. Dulya *et al.*, Nucl. Instrum. Meth. **A398**, 109 (1997).

[12] S. L. Bueltmann *et al.*, Nucl. Instrum. Meth. **A425**, 23 (1999).